Online-Journals.org

iJOE International Journal of Online and Biomedical Engineering

iJOE | eISSN: 2626-8493 | Vol. 21 No. 11 (2025) | OPEN ACCESS

https://doi.org/10.3991/ijoe.v21i11.56677

PAPER

Disturbance Observer-Based Sliding Mode Control for Ventilation Blower-Based Systems: Controller Design and Simulation

Cong Toai Truong[1,2], **Trung Dat Phan**[1,2], **Minh Tri Tran**[1,2], **Huy Hung Nguyen**[3], **Van Tu Duong**[1,2], **Tan Tien Nguyen**[1,2](✉)

[1]Ho Chi Minh University of Technology (HCMUT), Ho Chi Minh City, Vietnam

[2]Vietnam National University Ho Chi Minh City, Ho Chi Minh City, Vietnam

[3]Faculty of Engineering and Technology, Saigon University, Ho Chi Minh City, Vietnam

nttien@hcmut.edu.vn

ABSTRACT

This paper presents a disturbance observer-based sliding mode control (DO-SMC) for a ventilation blower-based system (VBS) to enhance control performance. Due to the complexity of physical modeling and the lack of blower specifications, the VBS model is approximated as a second-order transfer function using a black-box system identification approach. Additionally, the VBS model was evaluated using the Nash-Sutcliffe model efficiency coefficient, achieving a fit of 92.77%. To validate the performance of DO-SMC, various simulation scenarios were conducted both in the absence and presence of disturbances. In the disturbance-free scenario, the VBS controller effectively tracked the desired air volume during the inspiratory cycle. However, this effect is less evident at the start of the cycle due to rotor inertia and electrical driver characteristics. Specifically, the simulation data showed a maximum deviation of approximately 47 ml under these conditions. In contrast, under ramp and square disturbances combined with random noise, the proposed controller significantly reduced the steady-state error and improved response time, even in the presence of system uncertainties. Additionally, slight chattering was observed in the control signal, attributed to the controller's attempts to compensate for abrupt system behavior changes. As a result, accurate estimation of the ramp and square disturbances contributed to enhanced overall control performance by mitigating their effects, even though some residual errors remained in the higher-order tracking dynamics due to system limitations.

KEYWORDS

sliding mode control, black box, identification, ventilation blower-based system, disturbance

1 INTRODUCTION

In the field of healthcare, a crucial challenge is making life-saving medical equipment, particularly mechanical ventilators (MV) [1–3], accessible during global health

Truong, C. T., Phan, T. D., Tran, M. T., Nguyen, H. H., Duong, V. T., Nguyen, T. T. (2025). Disturbance Observer-Based Sliding Mode Control for Ventilation Blower-Based Systems: Controller Design and Simulation. *International Journal of Online and Biomedical Engineering (iJOE)*, 21(11), pp. 132–151. https://doi.org/10.3991/ijoe.v21i11.56677

Article submitted 2025-05-17. Revision uploaded 2025-07-15. Final acceptance 2025-07-15.

emergencies [4–5]. Specifically, the MVs support patients with respiratory failure, considerably improving survival rates in critical conditions [6]. Throughout history, pandemics such as the 1918 influenza and, more recently, COVID-19 have emphasized the urgent need for scalable solutions [7]. During the COVID-19 pandemic, the overwhelming demand for MVs exposed vulnerabilities in global healthcare infrastructure, especially in low-resource settings where supply chain disruptions and limited accessibility were prevalent [8–11]. These challenges underscore the importance of developing cost-effective MVs not only for basic functions but also for diverse patient populations under varying clinical conditions [12]. Consequently, this underscores the necessity of developing suitable control algorithms capable of effectively addressing external disturbances and system uncertainties to ensure efficient and reliable operation.

In recent years, numerous studies have focused on the development of advanced control strategies to address the challenges associated with ventilation blower-based systems (VBS) [13–15]. Among these challenges, achieving robustness, precise tracking performance, and adaptability in the presence of uncertainties, as well as external disturbances, has been considered significantly important [15]. In reality, the controllers have to maintain reliable performance across a wide range of clinical scenarios given the dynamic and patient-specific nature of respiratory mechanics, including inter-patient variability, varying airway resistances, spontaneous breathing efforts, and system perturbations [16]. Hence, several control methodologies have been explored, each addressing specific limitations of traditional controllers and contributing uniquely to the advancement of respiratory support systems.

Firstly, sliding mode control (SMC) has been extensively studied due to its robustness against model uncertainties and external disturbances [17]. Notably, SMC guarantees asymptotic tracking despite parameter variations by enforcing system trajectories to converge and remain on a predefined sliding manifold [15]. Expressly, it exhibits inherent insensitivity to bounded uncertainties, which makes it a potential candidate for systems with unknown or variable dynamics. However, traditional SMC suffers from the problem of the chattering phenomenon caused by high-frequency switching [18], which not only introduces steady-state oscillations but also poses practical limitations in sensitive medical contexts like MV [19]. Consequently, chattering can lead to pressure fluctuations, patient discomfort, or even injury, necessitating updated or combined control variants.

Additionally, model predictive control (MPC) offers a fundamentally different approach by solving an optimization problem at each time step to determine control actions based on future predictions [20]. This forward-looking nature allows MPC to handle multivariable objectives and constraints explicitly [21], making it suitable for respiratory systems where pressure, volume, and flow limits must be respected to avoid lung injury. MPC's ability to incorporate the prediction of patient effort and system dynamics enhances patient-ventilator synchrony [22]. Notwithstanding, its real-time implementation demands significant computational resources and relies heavily on model accuracy [23]. In the presence of patient-specific uncertainties or abrupt changes in dynamics, such as spontaneous breathing or airway occlusions, prediction errors can degrade control performance, raising safety and reliability concerns.

Besides, adaptive control strategies, such as model reference adaptive control (MRAC) and adaptive backstepping, are attractive due to their ability to estimate and compensate for uncertain parameters [24]. In the first place, MRAC adjusts itself based on the discrepancy between the plant output and a desired reference

model [25]. In general, when applied to MV, MRAC enables the system to accommodate variations in respiratory system parameters, including compliance and resistance, across different patients [26]. Nonetheless, MRAC typically requires measuring or estimating internal variables, as illustrated in MV, where the alveolar pressure may not be directly accessible in clinical settings. On the other hand, adaptive backstepping provides a systematic design procedure for nonlinear systems by recursively constructing virtual control inputs and associated Lyapunov functions. From there, it allows parameter adaptation while ensuring system stability [27]. Nevertheless, both methods may show degraded performance under external disturbances or modeling mismatches not captured by parameter uncertainty.

Intelligent control methods, particularly reinforcement learning (RL) and fuzzy logic control (FLC), represent a data-driven paradigm shift in MV control [28]. RL formulates the control problem as a Markov Decision Process, allowing the system to learn optimal ventilation policies via interaction and feedback. Advanced RL algorithms can operate without explicit plant models, relying instead on data to approximate optimal control strategies [29]. In intensive care datasets, RL-based frameworks like VentAI [30] have outperformed conventional strategies in optimizing ventilator settings for patient outcomes [31]. In contrast, RL's clinical applicability is constrained by its need for extensive training data and the risk associated with exploration in live patients. On the other hand, FLC encodes expert knowledge into a rule-based system using linguistic variables. It provides a robust solution to systems with ambiguous, nonlinear, or poorly defined models, as commonly seen in respiratory care [32]. Although FLC is easier to implement and interpret, it lacks formal stability guarantees and often requires empirical tuning of membership functions and rules, limiting its scalability and reproducibility.

Remarkably, active disturbance rejection control (ADRC) has emerged as a compelling alternative, particularly for systems with unmodeled dynamics or unknown disturbances [33]. ADRC introduces an extended state observer (ESO) to estimate the total disturbance, including model uncertainties and external perturbations, and employs a compensation control law to cancel it in real-time. In MV applications, ADRC has demonstrated improved pressure tracking and robustness without relying on accurate patient models [34]. Studies show that ADRC-equipped MVs achieve performance comparable to commercial systems while offering resilience to patient variability and system disturbances. Yet, ADRC's effectiveness hinges on proper tuning of observer and control gains, and its implementation complexity may hinder clinical deployment without streamlined calibration procedures.

Toward a unified and robust control framework, this paper proposes a promising approach: disturbance observer-based sliding mode control (DO-SMC) [35]. This method combines the robustness and finite-time convergence of sliding mode control (SMC) with the disturbance estimation capability of a disturbance observer (DO), thereby enhancing disturbance rejection while reducing the need for high switching gains [36]. Of which, DO-SMC does not require prior knowledge of disturbance bounds, making it well-suited for respiratory control under uncertain and time-varying conditions. Furthermore, the proposed DO-SMC framework integrates key advantages from both classical and modern control strategies. It incorporates the robustness of SMC, the disturbance estimation from active disturbance rejection control (ADRC), and the adaptability to changing patient conditions typically found in adaptive control methods [37]. In this study, the performance of the DO-SMC controller was evaluated through simulations under two conditions: without external

disturbances and with external disturbances. Based on the analysis of these scenarios, the main contributions of this paper are as follows:

- Designing and implementing a novel DO-SMC strategy that combines sliding mode control and disturbance observation strengths to improve robustness and accuracy under dynamic conditions.
- Extensive simulations were conducted to evaluate the control performance of the proposed method under scenarios with and without disturbances, demonstrating its superiority over conventional control strategies.

2 METHODOLOGY

The dynamic characteristics of a VBS can be described with a third-order state-space model as follows:

$$\begin{aligned} \dot{\boldsymbol{x}}(t) &= \boldsymbol{A}\boldsymbol{x}(t) + \boldsymbol{B}u(t), \\ y(t) &= \boldsymbol{C}\boldsymbol{x}(t), \end{aligned} \tag{1}$$

where $\boldsymbol{x}(t) \triangleq [V(t) \quad \dot{V}(t) \quad \ddot{V}(t)]^T$ is the state vector, $V(t)$ is the output air volume of the blower, $u(t)$ is the control signal, and the matrices

$$\boldsymbol{A} = \begin{bmatrix} 0 & 1 & 0 \\ 0 & 0 & 1 \\ 0 & -a_1 & -a_2 \end{bmatrix}, \boldsymbol{B} = \begin{bmatrix} 0 \\ 0 \\ h \end{bmatrix}, \boldsymbol{C} = \begin{bmatrix} 1 & 0 & 0 \end{bmatrix}, \tag{2}$$

where a_1, a_2 and h are determined by system identification.

Sampling the output of the system in Eq. (1) with a period T_s and applying the control signal using a zero-order hold (ZOH), the system plant can be represented in discrete time, including the disturbance $d(k)$. This disturbance includes the resistance force acting on the blower blade and the uncertainties in model identification. Assuming these uncertainties satisfy the matching condition, the discrete state-space model can be presented as follows:

$$\begin{aligned} \boldsymbol{x}(k+1) &= \boldsymbol{A}_{\boldsymbol{d}}\boldsymbol{x}(k) + \boldsymbol{B}_{\boldsymbol{d}}[u(k) + d(k)], \\ y(k) &= \boldsymbol{C}\boldsymbol{x}(k), \end{aligned} \tag{3}$$

in which the matrices

$$\begin{aligned} \boldsymbol{A}_{\boldsymbol{d}} &= \boldsymbol{I} + \sum_{k=1}^{\infty} \frac{\boldsymbol{A}^k T_s^k}{k!}, \\ \boldsymbol{B}_{\boldsymbol{d}} &= \sum_{k=0}^{\infty} \frac{\boldsymbol{A}^k T_s^k}{(k+1)!} T_s \boldsymbol{B}, \end{aligned} \tag{4}$$

are calculated computationally. $\boldsymbol{I} \in \mathbb{R}^{3\times 3}$ is the identity matrix, and the state vector in a discrete-time domain is defined by $\boldsymbol{x}(k) \triangleq [V(k) \quad \dot{V}(k) \quad \ddot{V}(k)]^T$. If the reference vector is $\boldsymbol{x}_{\boldsymbol{d}}(k) \triangleq [V_d(k) \quad \dot{V}_d(k) \quad \ddot{V}_d(k)]^T$, then the tracking error vector is defined by $\boldsymbol{e}(k) \triangleq \boldsymbol{x}(k) - \boldsymbol{x}_{\boldsymbol{d}}(k)$. The sliding variable can be chosen as

$$s(k) = \boldsymbol{c}^T \boldsymbol{e}(k), \tag{5}$$

where $\boldsymbol{c} \triangleq [\lambda^2 \quad 2\lambda \quad 1]^T$ is the sliding design parameter. The sliding variable at $k+1$ interval is given by

$$s(k+1) = \boldsymbol{c}^T \boldsymbol{e}(k+1). \tag{6}$$

From the system is described as Eq. (3), the definition of $e(k)$, and Eq. (6) follow as

$$s(k+1) = \boldsymbol{c}^T(\boldsymbol{A}_d \boldsymbol{x}(k) + \boldsymbol{B}_d u(k) + \boldsymbol{B}_d d(k) - \boldsymbol{x}_d(k+1)). \tag{7}$$

The control signal $u(k)$ consists of two components: the equivalent control u_e and the disturbance compensation u_c. The equivalent control can be obtained from nominal model of the system as Eq. (3) with Gao's reaching law condition $s(k+1) = \beta s(k) - \eta \text{sgn}(s(k))$ according to [38]. The equivalent control can be derived as

$$u_e(k) = (\boldsymbol{c}^T \boldsymbol{B}_d)^{-1}[\boldsymbol{c}^T \boldsymbol{x}_d(k+1) - \boldsymbol{c}^T \boldsymbol{A}_d \boldsymbol{x}(k) + \beta s(k) - \eta \text{sgn}(s(k))], \tag{8}$$

where $0 < \beta < 1$, $\eta > 0$ are designed positive constant. The term $\boldsymbol{c}^T \boldsymbol{B}_d$ is a nonzero scalar and can be proven based on Eq. (4) and the definition of $\boldsymbol{c}$.

$$\boldsymbol{c}^T \boldsymbol{B}_d = \boldsymbol{c}^T \left(T_s \boldsymbol{B} + \frac{T_s^2}{2} \boldsymbol{A}\boldsymbol{B} + \frac{T_s^3}{6} \boldsymbol{A}^2 \boldsymbol{B} + \cdots + \lim_{k \to \infty} \frac{T_s^{k+1}}{(k+1)!} \boldsymbol{A}^k \boldsymbol{B} \right). \tag{9}$$

Eq. (9) is equivalent to:

$$\boldsymbol{c}^T \boldsymbol{B}_d = h \begin{pmatrix} T_s + \frac{T_s^2}{2}(2\lambda - a_2) \\ + \frac{T_s^3}{6}(\lambda^2 - 2\lambda a_2 + a_2^2 - a_1) + \cdots + \lim_{k \to \infty} \frac{T_s^{k+1}}{(k+1)!} \boldsymbol{A}^k \end{pmatrix}. \tag{10}$$

It is easy to observe that with a sufficiently small T_s, the higher-order expansion terms in Eq. (10) tend to zero as $k \to \infty$. Consequently, with appropriately chosen λ and T_s, and given that $h \neq 0$, the term $\boldsymbol{c}^T \boldsymbol{B}_d$ is non-singular and the control law $u_e(k)$ is fully determined. To eliminate the disturbance $d(k)$, u_c is designed as

$$u_c(k) = -\hat{d}(k), \tag{11}$$

where $\hat{d}(k)$ is the estimation of external disturbance. The total control signal is defined by

$$u(k) = (\boldsymbol{c}^T \boldsymbol{B}_d)^{-1}[\boldsymbol{c}^T \boldsymbol{x}_d(k+1) - \boldsymbol{c}^T \boldsymbol{A}_d \boldsymbol{x}(k) + \beta s(k) - \eta \text{sgn}(s(k))] - \hat{d}(k). \tag{12}$$

Substituting Eq. (12) into Eq. (7), it can be obtained

$$s(k+1) = \beta s(k) - \eta \text{sgn}(s(k)) + \mu(k), \tag{13}$$

where $\mu(k) \triangleq \boldsymbol{c}^T \boldsymbol{B}_d \tilde{d}(k)$. Let $\tilde{d}(k) \triangleq d(k) - \hat{d}(k)$ is the disturbance prediction error, the disturbance estimation law $\hat{d}(k)$ can be designed according to [39], that is

$$\hat{d}(k) = \hat{d}(k-1) + (\boldsymbol{c}^T \boldsymbol{B}_d)^{-1} \alpha [s(k) - \beta s(k-1) + \eta \text{sgn}(s(k-1))], \tag{14}$$

where $0 < \alpha < 1$ is positive constant.

The prediction error dynamic can be obtained from Eqs. (13) and (14)

$$\tilde{d}(k+1) = d(k+1) - d(k) + (1-\alpha)\tilde{d}(k). \tag{15}$$

With a sufficiently small sampling time, there exists a value m. If the change rate of the disturbance satisfies $|d(k+1)-d(k)|<m$, the disturbance prediction error remains bounded and satisfies $|\tilde{d}(k)|<m/\alpha$ under the control law in Eq. (12) and disturbance observer shows as Eq. (14). If m is sufficiently small, this error will converge to zero following to [40].

With $0<|\mu(k)|<\boldsymbol{c}^T\boldsymbol{B}_d m\alpha^{-1}<\eta$, four conditions are analyzed to prove the stability of the system under the control laws in Eqs. (12) and (14).

- When $s(k)\geq \boldsymbol{c}^T\boldsymbol{B}_d(m/\alpha)+\eta>0$, it leads to

$$\begin{aligned} s(k+1)-s(k) &= (\beta-1)s(k)-\eta+\mu(k)\\ &\leq (\beta-1)\left(\frac{\boldsymbol{c}^T\boldsymbol{B}_d m}{\alpha}+\eta\right)-\eta+\mu(k)<0,\\ s(k+1)+s(k) &= (\beta+1)s(k)-\eta+\mu(k)\\ &> \frac{\boldsymbol{c}^T\boldsymbol{B}_d m}{\alpha}+\mu(k)>0. \end{aligned}$$

  It follows that,

$$|s(k+1)|\leq|s(k)|.$$

- When $s(k)\leq -\boldsymbol{c}^T\boldsymbol{B}_d(m/\alpha)-\eta<0$, it causes

$$\begin{aligned} s(k+1)-s(k) &= (\beta-1)s(k)+\eta+\mu(k)\\ &\geq (\beta-1)\left(-\frac{\boldsymbol{c}^T\boldsymbol{B}_d m}{\alpha}-\eta\right)+\eta+\mu(k)>0,\\ s(k+1)+s(k) &= (\beta+1)s(k)+\eta+\mu(k)\\ &< -\frac{\boldsymbol{c}^T\boldsymbol{B}_d m}{\alpha}+\mu\ (k)<0, \end{aligned}$$

  which implies that,

$$|s(k+1)|\leq|s(k)|.$$

- When $0<s(k)<\boldsymbol{c}^T\boldsymbol{B}_d(m/\alpha)+\eta$, this results in

$$\begin{aligned} s(k+1) &= \beta s(k)-\eta+\mu(k)\\ &< \beta\left(\frac{\boldsymbol{c}^T\boldsymbol{B}_d m}{\alpha}+\eta\right)+\mu(k)-\eta\\ &< \frac{\boldsymbol{c}^T\boldsymbol{B}_d m}{\alpha}+\mu(k)\\ &< \frac{\boldsymbol{c}^T\boldsymbol{B}_d m}{\alpha}+\eta,\\ s(k+1) &= \beta s(k)-\eta+\mu(k)\\ &> \mu(k)-\eta\\ &> -\frac{\boldsymbol{c}^T\boldsymbol{B}_d m}{\alpha}-\eta. \end{aligned}$$

It yields that,

$$\left|s(k+1)\right| < \frac{\boldsymbol{c}^T \boldsymbol{B}_d m}{\alpha} + \eta.$$

- When $-\boldsymbol{c}^T \boldsymbol{B}_d (m/\alpha) - \eta < s(k) < 0$, this yields

$$\begin{aligned} s(k+1) &= \beta s(k) + \eta + \mu(k) \\ &< \eta + \mu(k) \\ &< \frac{\boldsymbol{c}^T \boldsymbol{B}_d m}{\alpha} + \eta, \\ s(k+1) &= \beta s(k) + \eta + \mu(k) \\ &> -\frac{\boldsymbol{c}^T \boldsymbol{B}_d m}{\alpha} - \eta + \eta + \mu(k) \\ &> -\frac{\boldsymbol{c}^T \boldsymbol{B}_d m}{\alpha} - \eta. \end{aligned}$$

It can obtain that,

$$\left|s(k+1)\right| < \frac{\boldsymbol{c}^T \boldsymbol{B}_d m}{\alpha} + \eta.$$

From the four analyses above, it can be concluded that

$$\text{When } \left|s(k)\right| \geq \boldsymbol{c}^T \boldsymbol{B}_d (m/\alpha) + \eta, \left|s(k+1)\right| < \left|s(k)\right|. \tag{16}$$

$$\text{When } \left|s(k)\right| < \boldsymbol{c}^T \boldsymbol{B}_d (m/\alpha) + \eta, \left|s(k+1)\right| < \boldsymbol{c}^T \boldsymbol{B}_d (m/\alpha) + \eta. \tag{17}$$

Conditions from Eqs. (16) and (17) ensures that $s(k) \to 0$ in the presence of disturbances. The sampling time should be sufficiently small and α should be appropriately chosen so that m exists and satisfies $m/\alpha \ll 1$. Since $\boldsymbol{c}^T \boldsymbol{B}_d m \alpha^{-1} < \eta$, η is chosen sufficiently small and makes $\boldsymbol{c}^T \boldsymbol{B}_d (m/\alpha) + \eta \ll 1$. Consequently, $s(k+1)$ converges within a boundary layer around zero, with the bounds defined by $\boldsymbol{c}^T \boldsymbol{B}_d (m/\alpha) + \eta$.

In practice, $u(k)$ is usually bounded by $u_0 > 0$ due to the voltage limit of the actuator. Then the control law can be defined as

$$u(k) = \begin{cases} 0 & if\ u(k) < 0 \\ u(k) & if\ 0 \leq u(k) < u_0 \\ u_0 & if\ u(k) \geq u_0 \end{cases}. \tag{18}$$

3 CASE STUDY: VENTILATION BLOWER-BASED SYSTEM

Prior to designing the control parameters, the nominal model of the VBS needs to be determined through system identification.

3.1 System identification of VBS

Due to the lack of detailed information regarding the blower's blade design and the electrical characteristics of the driver, physically modeling the VBS becomes

challenging and complex. Therefore, the black-box system identification approach is employed in this study.

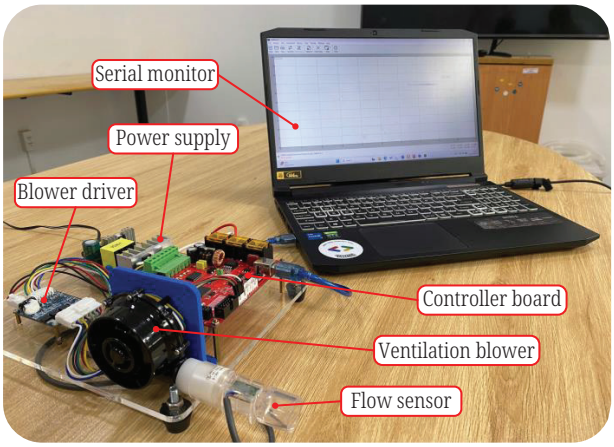

Fig. 1. Experimental setup of VBS for system identification

The data acquisition system for system identification is shown in Figure 1, consisting of a controller board, ventilation blower, flow sensor, blower driver, power supply, and serial monitor. The controller board regulates the blower's rotational speed via a PWM signal sent to the driver. The airflow generated by the blower is measured using an SFM3300 flow sensor. This data is transmitted to the controller board via I2C communication and subsequently sent to a computer through a serial connection. To determine the transfer function of the driver-blower system, input signals are applied to the driver while measuring the corresponding output values. The input signal is the PWM bit signal ranging from 0 to 255, while the output signal is the airflow at the blower's outlet, measured in ml/s. Two different input-output datasets are collected: one for system identification and another for validation. Both datasets are sampled at 500 Hz, with the input signal following a multi-step function comprising five voltage levels, each maintained for 3 s, as illustrated in Figure 2.

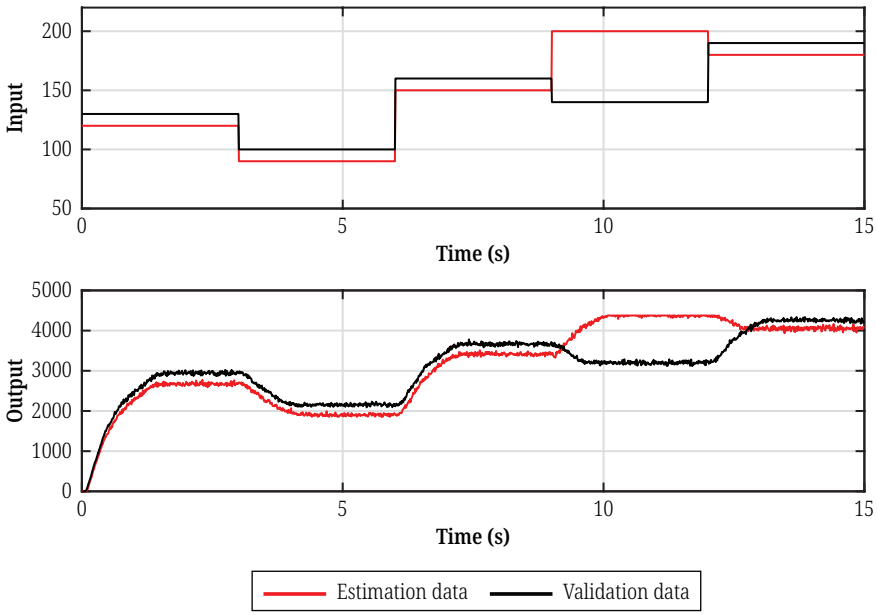

Fig. 2. Estimation and validation data of the VBS

Since the blower operates by adjusting the rotational speed of a brushless DC motor to generate airflow, the system's order is expected to be either first or second order. System identification was performed using both first- and second-order transfer functions, with the results shown in Figure 3. In this study, the Nash–Sutcliffe Efficiency (*NSE*) is employed to evaluate the goodness-of-fit between the identified model and the actual system response [41]. The reason for using *NSE* is that it is particularly suitable for assessing dynamic systems such as VBS, as it accounts for the entire time-series behavior rather than point-wise error alone [42]. Unlike other metrics, *NSE* provides a normalized, dimensionless metric that reflects how well the model predicts relative to the mean of observed data [43]. This allows for a more intuitive and robust comparison between first- and second-order models, making *NSE* a suitable choice. Therefore, the similarity between the estimated model output and the actual system response is evaluated using the *NSE*, given by the following formula:

$$NSE = 1 - \frac{\sum_{k=1}^{N_s} (y_k - \hat{y}_k)^2}{\sum_{k=1}^{N_s} (y_k - \bar{y})^2}, \tag{19}$$

where N_s is the number of samples; y_k is the *kth* data point of the reference dataset; $\hat{y}_k$ is the *kth* data point of the experimental dataset; $\bar{y}$ is the mean value of the reference dataset. It is evident that the second-order transfer function demonstrated better accuracy, achieving a 92.77% fit with the actual data, compared to 89.96% for the first-order model.

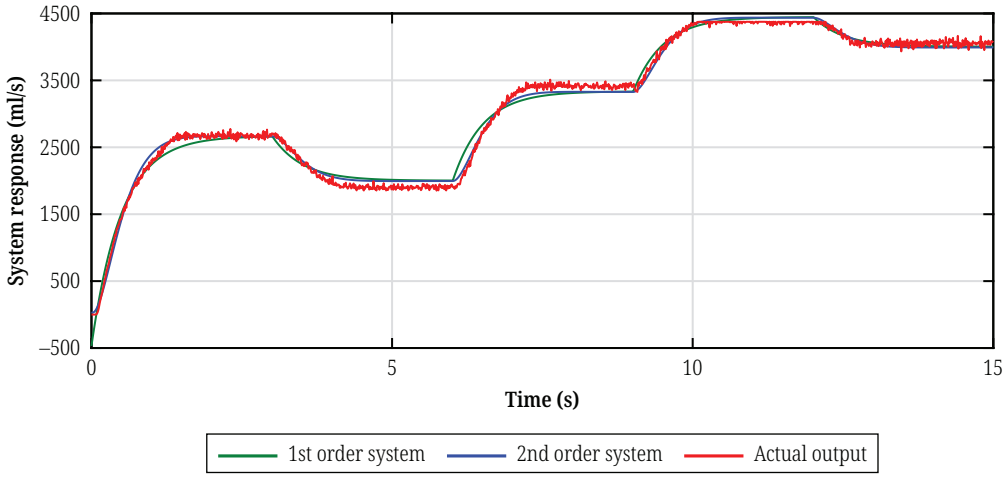

Fig. 3. Comparison of system response with first-order and second-order system estimation

Therefore, the transfer function of the VBS is approximated as a second-order transfer function, expressed as follows:

$$G(s) = \frac{Q(s)}{U(s)} = \frac{267.9}{s^2 + 6.253s + 12.08}, \tag{20}$$

where $Q(s)$ is the airflow output; $U(s)$ is the control signal.

The second dataset is used to evaluate the suitability of the transfer function as Eq. (17) for different input signal levels. The calculated *NSE* value in this case

is 90.56%. Therefore, the transfer function shown in Eq. (20) can be utilized for designing the controller for the VBS. For an output representing air volume, the transfer function in Eq. (20) is rewritten in state-space form as shown in Eq. (1) with the matrices

$$\boldsymbol{A}=\begin{bmatrix}0 & 1 & 0\\ 0 & 0 & 1\\ 0 & -12.08 & -6.253\end{bmatrix},\ \boldsymbol{B}=\begin{bmatrix}0\\ 0\\ 267.9\end{bmatrix},\ \boldsymbol{C}=\begin{bmatrix}1 & 0 & 0\end{bmatrix}. \tag{21}$$

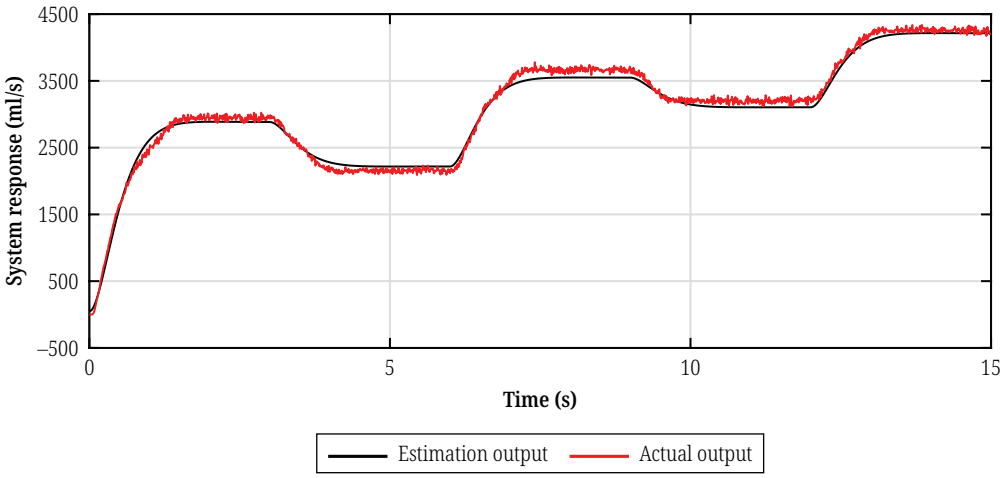

Fig. 4. The validation result of the second-order transfer function model using an independent dataset

Figure 4 presents the validation result of the second-order transfer function model using an independent dataset. The input signal comprises multiple step changes in control voltage, and the system's airflow response is compared between the estimated model and the actual measured output. It can be seen that the estimated model accurately replicates the system's dynamic behavior across all input levels. The model captures both the transient response and steady-state values with high fidelity. Minor deviations are observed during the fast transitions, likely due to unmodeled nonlinearities or actuator saturation, but these discrepancies remain within acceptable margins. Therefore, the validated second-order model is well-suited for subsequent controller design in the VBS.

3.2 Simulation results

The proposed control algorithm is validated through computational simulation before being applied to the physical system. In this case study, the behavior of the VBS is simulated to mimic the periodic volume control process of blower-based ventilators. A single cycle consists of two phases: the inspiratory and expiratory phases. The inspiratory phase lasts for $\boldsymbol{T_i}$, while the expiratory one lasts for $\boldsymbol{T_e}$. During the pumping phase, the volume is controlled to follow a ramp profile, reaching a maximum tidal volume $\boldsymbol{V_T}$ at the end of this phase. In the expiratory phase, the pump remains inactive, allowing passive air release over $\boldsymbol{T_e}$, before a new cycle begins. The parameter settings are chosen as: $\boldsymbol{V_T = 500\ ml}$, $\boldsymbol{T_i = 1\ s}$, $\boldsymbol{T_e = 2\ s}$, $\boldsymbol{T_s = 0.002\ s}$, $\boldsymbol{\lambda = 4.8}$, $\boldsymbol{\alpha = 0.99}$, $\boldsymbol{\beta = 0.99}$, $\boldsymbol{\eta = 0.0052}$, $\boldsymbol{u_0 = 255}$. The initial values of the state vector

and disturbance estimation are chosen as $\boldsymbol{x}(\mathbf{0}) = \begin{bmatrix}\mathbf{0} & \mathbf{0} & \mathbf{0}\end{bmatrix}^T$, $\hat{\boldsymbol{d}}(\mathbf{0}) = \mathbf{0}$. The matrices $\boldsymbol{A}_d$ and $\boldsymbol{B}_d$ after the discretization process, are

$$\boldsymbol{A}_d = \begin{bmatrix}\mathbf{1} & \mathbf{0.002} & \mathbf{0} \\ \mathbf{0} & \mathbf{1} & \mathbf{0.002} \\ \mathbf{0} & \mathbf{-0.0240} & \mathbf{0.9875}\end{bmatrix}, \quad \boldsymbol{B}_d = \begin{bmatrix}\mathbf{0} \\ \mathbf{0} \\ \mathbf{0.7312}\end{bmatrix}.$$

Case 1: VBS without disturbance

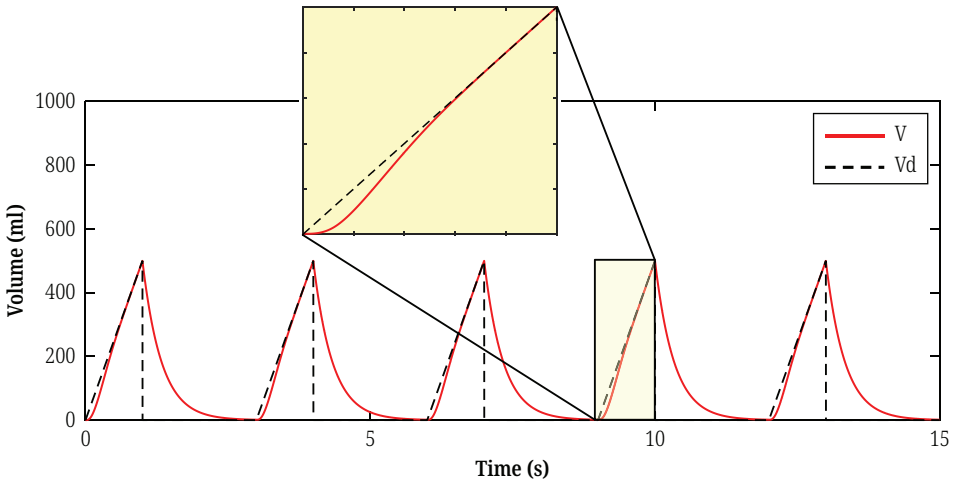

Fig. 5. The response of the VBS in tracking a ramp reference air volume under disturbance-free conditions

Figure 5 shows the response of the VBS in tracking a ramp reference air volume under disturbance-free conditions. The system demonstrates accurate tracking during the second half of the cycle, indicating that the controller can stabilize airflow after initial transients. However, a significant tracking error occurs in the first half of the cycle, with a maximum deviation of approximately 47 ml. This discrepancy is primarily due to motor inertia, which delays the rise in rotational speed required to produce airflow, and the limited range of control signals, which constrains the system's ability to follow the reference immediately. Despite these initial limitations, the air volume output converges smoothly to the desired trajectory in the latter part of the cycle. This result suggests that the proposed controller ensures reliable steady-state tracking.

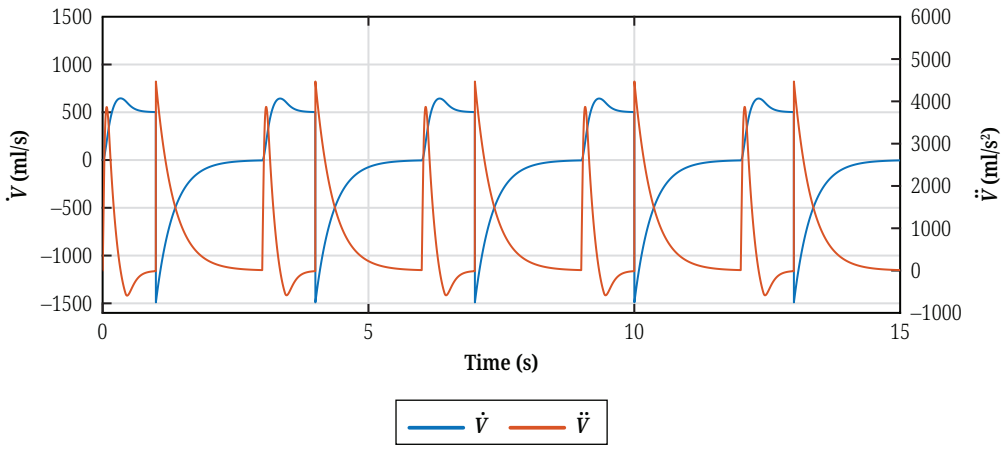

Fig. 6. The time responses of the system's internal state variables $\dot{V}$ and $\ddot{V}$ for the VBS without any external disturbance

Figure 6 depicts the time responses of the system's internal state variables $\dot{V}$ and $\ddot{V}$ for the VBS without any external disturbance. The second state variable, $\dot{V}$, represents the airflow rate, which quantifies the rate of change of air volume over time and is measured in milliliters per second (ml/s). The third state variable, $\ddot{V}$, denotes the acceleration of airflow, corresponding to the rate of change of the airflow rate, and is expressed in milliliters per second squared (ml/s^2). Both state variables remain well-bounded within safe limits throughout the operation, indicating that the closed-loop system maintains stable internal dynamics. During the active inspiratory phase, $\dot{V}$ and $\ddot{V}$ exhibit only moderate transient fluctuations and quickly settle into a repeatable pattern with each subsequent cycle.

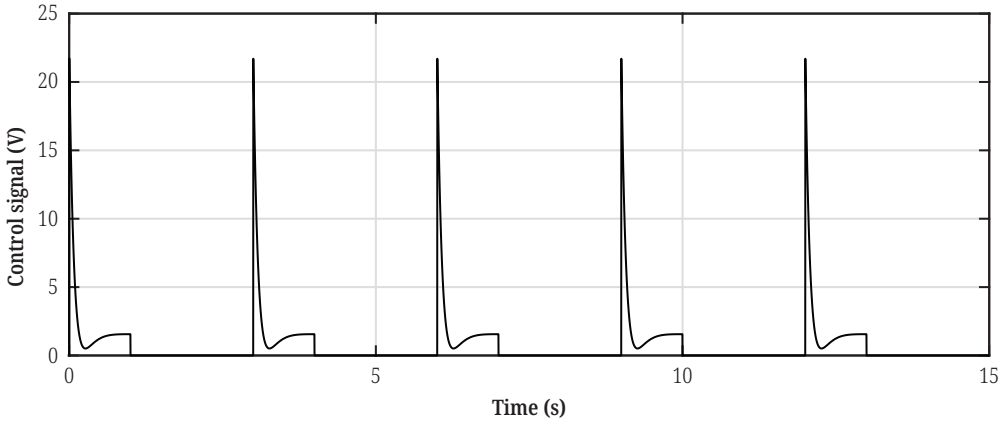

Fig. 7. The control input signal applied to the VBS in the absence of disturbances

Figure 7 presents the control input signal applied to the VBS in the absence of disturbances. Throughout the breathing cycle, the control effort varies smoothly without any high-frequency chattering or abrupt changes. At the start of the inspiratory cycle, the controller outputs a high command to accelerate airflow and track the ramp volume reference rapidly, then gradually reduces the input as the target volume approaches. During the expiratory cycle, the control signal returns to zero, reflecting the pump's inactive period and allowing passive exhalation. The absence of oscillatory control action indicates a well-tuned sliding mode controller that meets the demand without inducing instability.

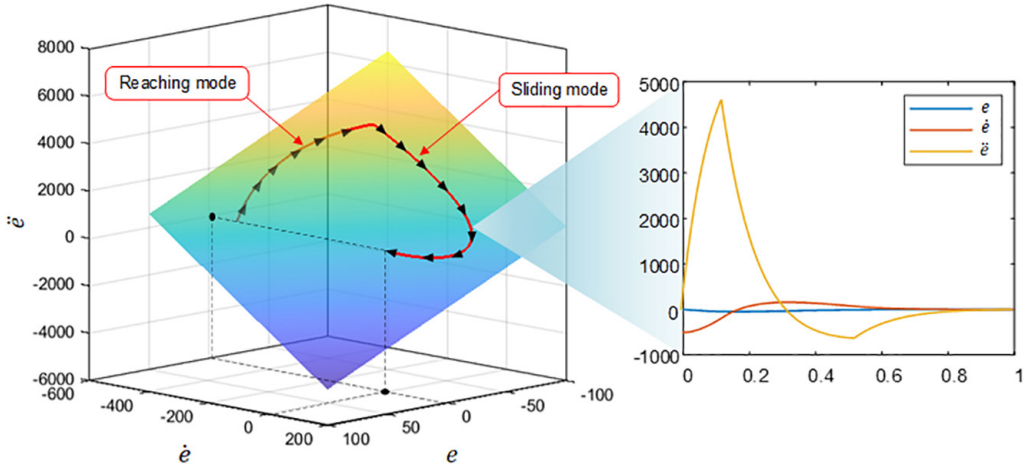

Fig. 8. The error dynamics of the VBS without disturbance

Figure 8 illustrates the phase trajectory of the system's error dynamics at the fifth cycle, where the system is assumed to have reached quasi-steady behavior [44], [45]. The plotted states include the tracking error $e(k)$, its first derivative $\dot{e}(k)$, and the second derivative $\ddot{e}(k)$. The trajectory exhibits a clear converging spiral toward the origin, showing that all components of the error dynamic tend toward zero. Specifically, the error amplitude reduces to below 5 ml, and the error derivative approaches near-zero within 0.2 seconds. These results demonstrate that the control laws defined in Eqs. (10) and (12) satisfy the Lyapunov stability condition, confirming that the sliding surface is attractive and invariant. Thus, the system exhibits asymptotic stability and convergence in higher-order dynamics, a key requirement for volume control in ventilation scenarios.

Case 2: VBS with external disturbance

In this case, ramp and square disturbances with random noise are considered, with the governing equation given by

$$d_{ramp}(t) = -\frac{5}{T_i}t + \epsilon_1, \quad \epsilon_1 \in [-0.2; 0.2], \tag{22}$$

$$d_{square}(t) = -10 + \epsilon_2, \quad \epsilon_2 \in [-0.5; 0.5], \tag{23}$$

where ϵ_1, ϵ_2 are random noise terms following a normal distribution.

The controller parameters remain unchanged from Case 1, and the control performance of the VBS in the presence of disturbances is illustrated in Figure 9 through Figure 13.

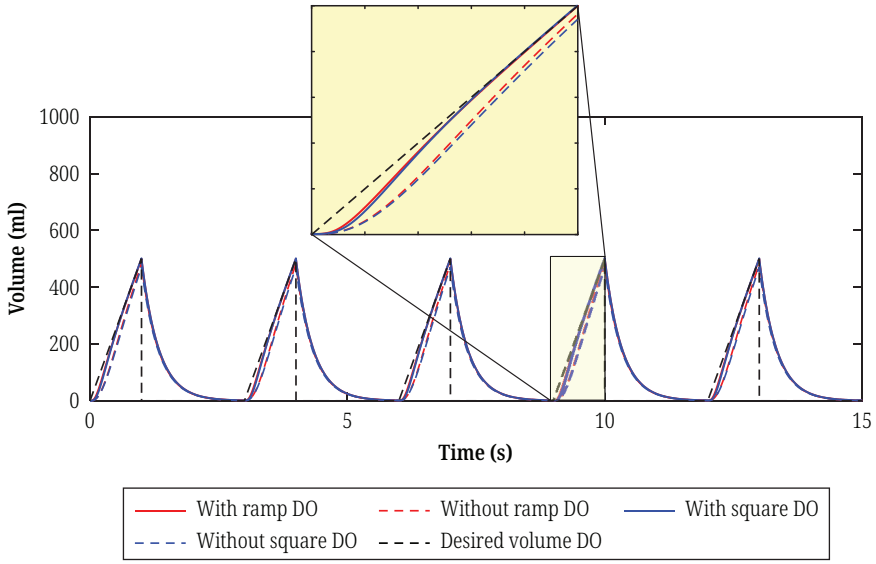

Fig. 9. Comparison of air volume response between the system with and without DO for noisy ramp and square disturbance

Figure 9 compares the volume tracking performance of the VBS with and without the disturbance observer under two types of external disturbances: a noisy ramp and a noisy square wave. In the presence of the ramp disturbance, the system without a disturbance observer exhibits a steady-state tracking error of up to 28 ml, and a visible lag in reaching the target volume. In contrast, the observer-based controller reduces this error to less than 5 ml, with much faster settling behavior. Similarly, under the square disturbance, the system without the observer shows large volume

deviations approximately to 25 ml immediately following each abrupt step. With the observer activated, these deviations are mitigated to within 4–6 ml, and the volume output more closely follows the reference trajectory. These results clearly demonstrate that the disturbance observer enhances system robustness and tracking precision under both gradual and abrupt disturbances, validating its role in maintaining performance in uncertain environments.

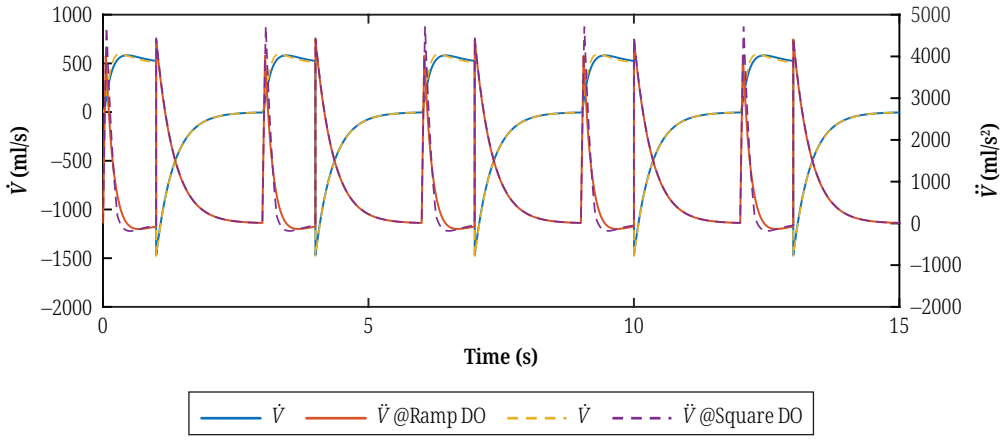

Fig. 10. $\dot{V}$ and $\ddot{V}$ response of the VBS with noisy ramp and square disturbance

Figure 10 presents the responses of the internal state variables $\dot{V}$ and $\ddot{V}$ for the VBS when subjected to the same noisy ramp and square disturbances. Despite the imposed perturbations, both $\dot{V}$ and $\ddot{V}$ remain bounded and follow behavior similar to that in the disturbance-free scenario. The state trajectories experience only small oscillations due to the injected noise, and these fluctuations are limited in magnitude without any tendency to grow unbounded. Each state variable preserves a consistent periodic pattern through each cycle's inspiratory and expiratory phases, indicating that the controller effectively manages the system's internal dynamics even under disturbance conditions. The fact that $\dot{V}$ and $\ddot{V}$ stay within acceptable limits confirms that the closed-loop system retains its stability and that the controller's robustness.

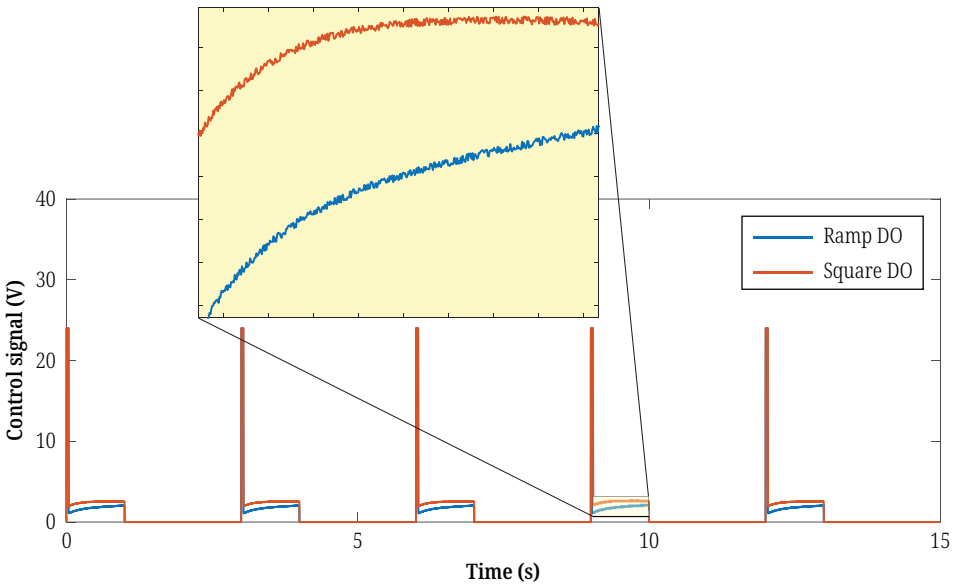

Fig. 11. Control signal of the VBS with noisy ramp and square disturbance

Notable differences appear in the control signal compared to the disturbance-free system. Specifically, in Figure 11, chattering occurs at the end of the inspiratory phase due to the presence of system noise. This phenomenon arises from the controller's attempt to counteract sudden variations in system behavior, which results in high-frequency oscillations in the control input. Nevertheless, the amplitude of these fluctuations remains within approximately one unit of $u(k)$, corresponding to 0.1 V. Aside from this minor jitter, the control input retains a largely smooth profile throughout the cycle, reflecting the system's overall resilience. The limited and low-amplitude nature of the chattering indicates that the disturbance observer effectively mitigates most of the noise impact, requiring only minimal corrective adjustments and thereby avoiding undue wear on the actuator.

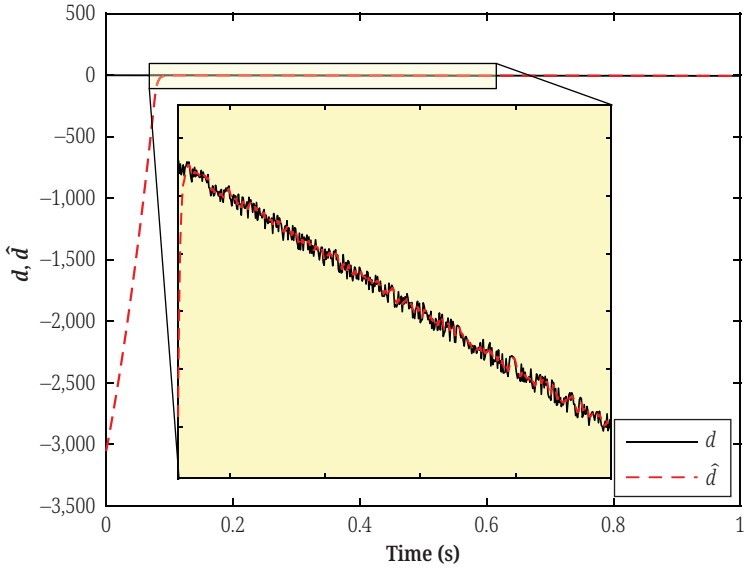

a) Disturbance observer output with noisy ramp disturbance

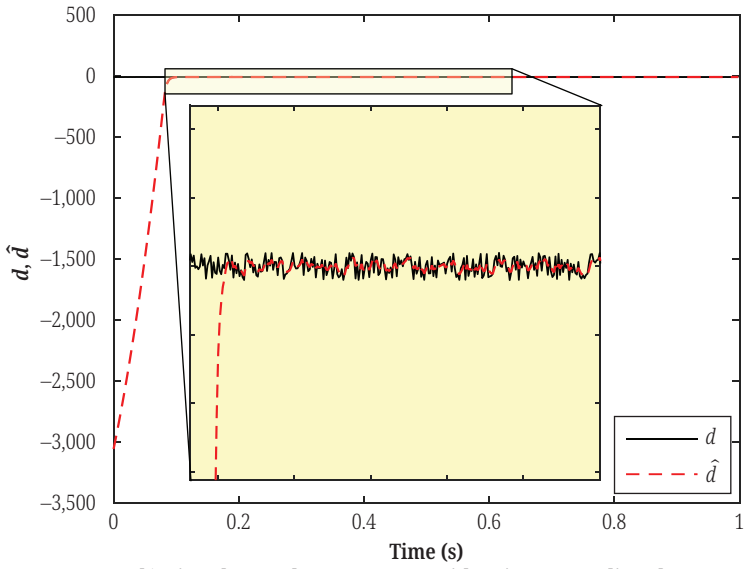

b) Disturbance observer output with noisy square disturbance

Fig. 12. Disturbance observer output with noisy ramp and square disturbance

The estimation of the ramp and square disturbances is illustrated in Figure 12. The black solid line represents the actual disturbance value, while the red dashed

line corresponds to the estimated disturbance. The estimation error decreases rapidly in both cases and converges to zero within 0.1 seconds. The accuracy of the disturbance estimation is closely related to the parameters m and α. A smaller sampling time improves the accuracy of the estimation, leading to better overall control performance. This accurate estimation is essential for feedforward compensation in the control loop, allowing the system to suppress the effect of unknown inputs in real time. The observer's performance demonstrates effectiveness across continuous and discontinuous disturbance types, ensuring stable and precise volume control under uncertain operating conditions.

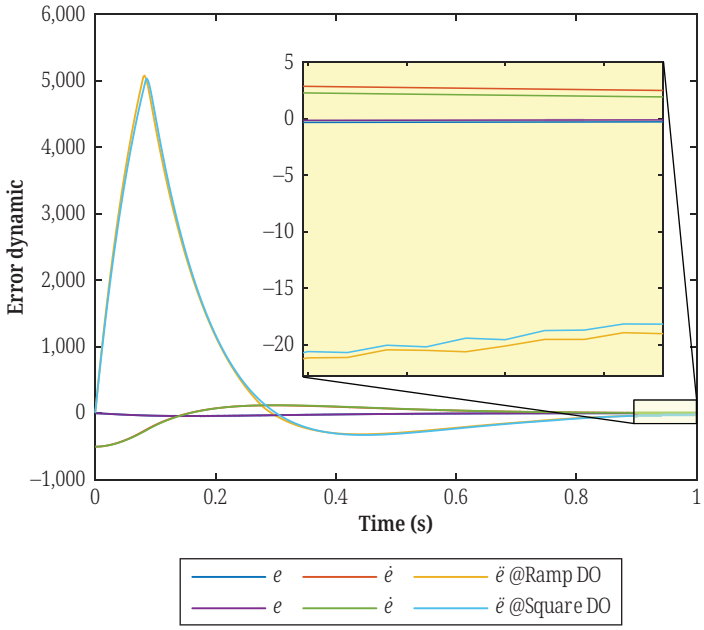

Fig. 13. The error dynamics of the VBS in the presence of a noisy ramp and a square disturbance

Figure 13 illustrates the error dynamics of the VBS under the influence of both ramp and square disturbances, including the tracking error $e(k)$, its first derivative $\dot{e}(k)$, and the second derivative $\ddot{e}(k)$. As shown, all three error components generally trend toward zero, indicating that the system is capable of attenuating the impact of external disturbances over time. Notably, while the position tracking error $e(k)$ converges effectively toward zero by the end of each inspiratory phase, and small residual errors remain in $\dot{e}(k)$ and $\ddot{e}(k)$. This behavior primarily results from the structure of the gain matrix c, which prioritizes the convergence of $e(k)$ by assigning it a dominant gain term λ^2, while assigning relatively smaller gains to its derivatives. For volume-based ventilation systems, accurate regulation of the tidal volume V_T is the principal control goal. Therefore, enforcing zero steady-state error in volume is critical, whereas allowing small steady-state values in derivative errors helps prevent excessive control effort and ensures smooth system response without compromising stability.

4 CONCLUSIONS

In summary, this paper presents the novel DO-SMC, which was proposed for VBS to enhance volume control performance. The method integrates the robustness of SMC with the disturbance compensation capabilities of a disturbance observer, which ensures better tracking accuracy, reduced steady-state error, and improved stability.

Moreover, the proposed controller outperformed traditional control methods through extensive simulations, particularly in handling disturbances and model uncertainties. The DO-SMC method demonstrated the ability to maintain precise pressure control even under challenging conditions, making it a promising solution for critical applications, where reliability and precision are of dramatic importance.

Future research on the DO-SMC method can build on this paper, conducting experiments in real-world conditions to validate its feasibility and reliability. Before large-scale deployment is also essential. Besides, the next workload can optimize the algorithm parameters to enhance performance and adaptability for more complex dynamic systems. Moreover, this method can incorporate artificial intelligence to improve its ability to auto-update the operation of this method in the real world.

5 ACKNOWLEDGMENT

This study is funded by Vietnam National University Ho Chi Minh City (VNU-HCM) under grant number TX2025-20b-01. We acknowledge the support of time and facilities from Key Laboratory of Digital Control and System Engineering (DCSELab), Ho Chi Minh City University of Technology (HCMUT), VNU-HCM for this study.

6 REFERENCES

[1] A. D. Afenigus and M. A. Sinshaw, "Ethical dilemmas and decision-making in emergency and critical care nursing in Western Amhara region, Northwest Ethiopia: A multi-method qualitative study," *BMC Nurs.*, vol. 24, 2025. https://doi.org/10.1186/s12912-025-02958-5

[2] C. T. Truong, D. K. Nguyen, N. Q. Tran, V. T. Duong, H. H. Nguyen, and T. T. Nguyen, "Applying the bilinear model to identify the ventilator's two double-acting pistons pump," in *9th International Conference on the Development of Biomedical Engineering in Vietnam. BME 2022, IFMBE Proceedings*, V. T. Vo, TH. Nguyen, B. L. Vong, N. B. Le, and T. Q. Nguyen, Eds., vol. 95, Springer, Cham, 2024, pp. 969–984. https://doi.org/10.1007/978-3-031-44630-6_77

[3] D. K. Nguyen, C. T. Truong, V. T. Duong, H. H. Nguyen, and T. T. Nguyen, "Model identification of two double-acting pistons pump," *Journal of Advanced Marine Engineering and Technology*, vol. 47, no. 2, pp. 59–65, 2023. https://doi.org/10.5916/jamet.2023.47.2.59

[4] H. González, C. J. Arizmendi, and B. F. Giraldo, "Development of a deep learning model for the prediction of ventilator weaning," *International Journal of Online and Biomedical Engineering (iJOE)*, vol. 20, no. 11, pp. 161–178, 2024. https://doi.org/10.3991/ijoe.v20i11.49453

[5] Q. Alyazji and G. Asiksoy, "Evaluating mechanical ventilators using multi criteria decision making techniques," *International Journal of Online and Biomedical Engineering (iJOE)*, vol. 17, no. 7, pp. 4–18, 2021. https://doi.org/10.3991/ijoe.v17i07.21769

[6] K. H. Huynh, C. T. Truong, T. D. Phan, V. T. Duong, H. H. Nguyen, and T. T. Nguyen, "A comparative study on estimated methods for airway resistance and lung compliance in air breath circuit," in *10th International Conference on the Development of Biomedical Engineering in Vietnam*, *BME 2024, IFMBE Proceedings*, V. T. Vo, T.-H. Nguyen, B. L. Vong, T. T. H. Pham, and N. H. Doan, Eds., vol. 122, Springer, Cham, 2025, pp. 324–333. https://doi.org/10.1007/978-3-031-90194-2_23

[7] E. Coulibali, J. Sadefo Kamdem, and C. Foguem, "A comparative analysis of the socio-economic and health impacts of three major pandemics: The Black Death, Spanish Flu, and Covid-19," HAL Open Science, 2025. [Online]. Available: https://hal.science/hal-04977730v1

[8] C. T. Truong *et al.*, "Model indentification of two double-acting pistons pump: A NARX network approach," in *2023 20th International Conference on Ubiquitous Robots (UR)*, 2023, pp. 771–778. https://doi.org/10.1109/UR57808.2023.10202388

[9] C. T. Truong, K. H. Huynh, V. T. Duong, H. H. Nguyen, L. A. Pham, and T. T. Nguyen, "Model free volume and pressure cycled control of automatic bag valve mask ventilator," *AIMS Bioeng.*, vol. 8, no. 3, pp. 192–207, 2021. https://doi.org/10.3934/bioeng.2021017

[10] C. T. Truong, K. H. Huynh, V. T. Duong, H. H. Nguyen, L. A. Pham, and T. T. Nguyen, "Linear regression model and least square method for experimental identification of AMBU bag in simple ventilator," *International Journal of Intelligent Unmanned Systems*, vol. 11, no. 3, pp. 378–395, 2023. https://doi.org/10.1108/IJIUS-07-2021-0072

[11] C. T. Truong, T. D. Phan, V. T. Duong, H. H. Nguyen, and T. T. Nguyen, "Model identification of ventilation air pump utilizing Ridge-momentum regression and Grid-based structure optimization," *Mathematical Biosciences and Engineering*, vol. 22, no. 8, pp. 2020–2038, 2025. https://doi.org/10.3934/mbe.2025074

[12] A. M. Valencia, I. Ruiz, J. I. García, and A. Galvis, "Design of a patient simulator for clinicians training in mechanical ventilation: SimVep," *J. Med. Eng. Technol.*, vol. 49, no. 3, pp. 79–92, 2025. https://doi.org/10.1080/03091902.2025.2484672

[13] T. D. Phan, L. X. Truong Pham, C. T. Truong, V. T. Duong, and H. H. Nguyen, "Adaptive sliding mode control for a blower-based breathing simulator with unknown and time-varying airway resistance and compliance," in *2024 International Conference on Engineering and Emerging Technologies (ICEET)*, 2024, pp. 1–6. https://doi.org/10.1109/ICEET65156.2024.10913788

[14] S. Saisukirtha, M. Omprakash, S. S. Steffy, and S. D. Kumar, "Smart ventilation bag with adjustable oxygen range and automated pressure regulation," in *2025 3rd International Conference on Intelligent Data Communication Technologies and Internet of Things (IDCIoT)*, 2025, pp. 1014–1019. https://doi.org/10.1109/IDCIOT64235.2025.10914958

[15] D. Acharya and D. K. Das, "A systematic review on state of modeling, clinical issues, and advanced control approaches for artificial ventilator: Traditional control to soft computing-based control approach," *Int. J. Dyn. Control*, vol. 13, 2024. https://doi.org/10.1007/s40435-024-01502-8

[16] A. Thankamony, S. Moideen, A. N. Shallik, R. B. Lloyd, H. A. Zaki, and N. A. Shallik, "The respiratory physics and mechanics of flow-controlled ventilation," in *Flow Controlled Ventilation Mode Through a Straw Size Tube*, N. A. Shallik, Ed., 2025, pp. 63–80. https://doi.org/10.1007/978-3-031-77477-5_5

[17] V. I. Utkin, *Sliding Modes in Control and Optimization*. Heidelberg: Springer Berlin, 1992. https://doi.org/10.1007/978-3-642-84379-2

[18] L. Zhang, L. Xiang, Z. Guangdeng, and W. Wang, "Kalman filter-based SMC for systems with noise and disturbances: Applications to magnetic levitation system," *Int. J. Syst. Sci.*, pp. 1–13, 2025. https://doi.org/10.1080/00207721.2025.2468364

[19] S. K. Spurgeon, "Sliding mode control: A tutorial," *IEE Proceedings Control Theory and Applications*, 1997. https://doi.org/10.1049/ic:19971292

[20] J. B. Rawlings and D. Q. Mayne, *Model Predictive Control: Theory and Design*. Madison, WI: Nob Hill Publishing, 2009.

[21] S. Kalaycioglu and A. de Ruiter, "Advanced control strategies for space systems: Integration of model predictive control and neural networks," in *Advances in Robust Control and Applications*, 2025. https://doi.org/10.5772/intechopen.1010037

[22] M. Akbari, "Patient-ventilator interaction optimization using MPC," *IFAC World Congress*, 2021.

[23] Z. Li, G. Dewantoro, T. Xiao, and A. Swain, "A comparative analysis of fuzzy logic control and model predictive control in photovoltaic maximum power point tracking," *Electronics*, vol. 14, no. 5, p. 1009, 2025. https://doi.org/10.3390/electronics14051009

[24] P. Ioannou and J. Sun, *Robust Adaptive Control*. Upper Saddle River, NJ: Prentice Hall, 1996.

[25] J. Du, S. Zhao, J. Wang, R. Yang, and A. Chang, "Active heave compensation for remotely operated vehicle recovery operations under random wave disturbances," *Physics of Fluids*, vol. 37, no. 3, p. 037160, 2025. https://doi.org/10.1063/5.0260044

[26] A. Sundaresan, "Adaptive control of pressure-controlled ventilation," in *IEEE Conference on Decision and Control*, 2019.

[27] M. Krstić, *Nonlinear and Adaptive Control Design*. New York, NY: Wiley, 1995.

[28] R. S. Sutton and A. G. Barto, *Reinforcement Learning: An Introduction*. Cambridge, MA: MIT Press, 2018.

[29] M. Komorowski *et al.*, "The artificial intelligence clinician learns optimal treatment strategies for sepsis in intensive care," *Nat. Med.*, vol. 24, pp. 1716–1720, 2018. https://doi.org/10.1038/s41591-018-0213-5

[30] C. Yin, R. Liu, J. Caterino, and P. Zhang, "Deconfounding actor-critic network with policy adaptation for dynamic treatment regimes," in *Proceedings of the ACM SIGKDD International Conference on Knowledge Discovery and Data Mining (KDD '22)*, Association for Computing Machinery, 2022, pp. 2316–2326. https://doi.org/10.1145/3534678.3539413

[31] A. Peine *et al.*, "Development and validation of a reinforcement learning algorithm to dynamically optimize mechanical ventilation in critical care," *npj Digit. Med.*, vol. 4, p. 32, 2021. https://doi.org/10.1038/s41746-021-00388-6

[32] L. A. Zadeh, "Fuzzy sets," Electronics Research Laboratory, University of Califonia, 1965. https://doi.org/10.21236/AD0608981

[33] J. Han, "From PID to active disturbance rejection control," *IEEE Transactions on Industrial Electronics*, vol. 56, no. 3, pp. 900–906, 2009. https://doi.org/10.1109/TIE.2008.2011621

[34] D. I. R. Almeida *et al.*, "Modeling and control of an invasive mechanical ventilation system using the active disturbances rejection control structure," *ISA Transactions*, vol. 129, pp. 345–354, 2021. https://doi.org/10.1016/j.isatra.2021.12.021

[35] D. Ginoya, P. D. Shendge, and S. B. Phadke, "Disturbance observer based sliding mode control of nonlinear mismatched uncertain systems," *Communications in Nonlinear Science and Numerical Simulation*, vol. 26, nos. 1–3, pp. 98–107, 2015. https://doi.org/10.1016/j.cnsns.2015.02.008

[36] O. Kaplan, F. Bodur, and M. B. Ozdemir, "Arbitrary fixed-time sliding mode control for buck converter with matched and mismatched disturbances based on fixed-time observer," *IEEE Access*, vol. 13, pp. 4582–4596, 2025. https://doi.org/10.1109/ACCESS.2024.3525092

[37] J. Wang, Q. Jiang, and R. Ibrahim, "Improved sliding mode active disturbance rejection control of an auxiliary robotic arm for puncture robots," *International Journal of Robust and Nonlinear Control*, vol. 35, no. 11, pp. 4826–4840, 2025. https://doi.org/10.1002/rnc.7945

[38] P. Latosiński and K. Adamiak, "Discrete-time sliding mode control strategies—State of the art," *Energies*, vol. 17, no. 18, p. 4564, 2024. https://doi.org/10.3390/en17184564

[39] L. Jinkun and W. Xinhua, *Advanced Sliding Mode Control for Mechanical Systems*. Heidelberg: Springer Berlin, 2012.

[40] Y. Eun, J. H. Kim, K. Kim, and D. Il Cho, "Discrete-time variable structure controller with a decoupled disturbance compensator and its application to a CNC servomechanism," *IEEE Transactions on Control Systems Technology*, vol. 7, no. 4, pp. 414–423, 1999. https://doi.org/10.1109/87.772157

[41] L. Duc and Y. Sawada, "A signal-processing-based interpretation of the Nash–Sutcliffe efficiency," *Hydrol. Earth Syst Sci*, vol. 27, no. 9, pp. 1827–1839, 2023. https://doi.org/10.5194/hess-27-1827-2023

[42] W. J. M. Knoben, J. E. Freer, and R. A. Woods, "Technical note: Inherent benchmark or not? Comparing Nash–Sutcliffe and Kling–Gupta efficiency scores," *Hydrol. Earth Syst. Sci.*, vol. 23, no. 10, pp. 4323–4331, 2019. https://doi.org/10.5194/hess-23-4323-2019

[43] L. A. Melsen, A. Puy, P. J. J. F. Torfs, and A. Saltelli, "The rise of the Nash-Sutcliffe efficiency in hydrology," *Hydrological Sciences Journal*, vol. 70, no. 8, pp. 1248–1259, 2025. https://doi.org/10.1080/02626667.2025.2475105

[44] W. Gao, Y. Wang, and A. Homaifa, "Discrete-time variable structure control systems," *IEEE Transactions on Industrial Electronics*, vol. 42, no. 2, pp. 117–122, 1995.

[45] S. Sarpturk, Y. Istefanopulos, and O. Kaynak, "On the stability of discrete-time sliding mode control systems," *IEEE Trans. Automat. Contr.*, vol. 32, no. 10, pp. 930–932, 1987. https://doi.org/10.1109/TAC.1987.1104468

7 AUTHORS

Cong Toai Truong received his B.E. degree from Mechatronics Engineering, University of Technology and Education Ho Chi Minh City, Vietnam in 2019, his M.S. degree from Mechatronics Engineering, Ho Chi Minh City University of Technology, Vietnam in 2021. His interest includes mechatronics, medical equipment, manufacturing design and industrial automation (E-mail: tctoai.sdh232@hcmut.edu.vn).

Trung Dat Phan received his B.E. degree from Mechatronics Engineering, Ho Chi Minh City University of Technology, Vietnam in 2023. His interest includes mechatronics, medical equipment, application control, and computer-aided engineering (E-mail: ptdat.sdh241@hcmut.edu.vn).

Minh Tri Tran started studying Mechatronics Engineering in Ho Chi Minh City University of Technology, Vietnam in 2020. His interest includes mechatronics, manufacturing processes and mechanical design (E-mail: tri.tranjusanban@hcmut.edu.vn).

Huy Hung Nguyen received the M.Sc. degree from Ho Chi Minh City University of Technology, Ho Chi Minh, Vietnam in 2001 and the Ph.D. degree in Mechanical Design Engineering from Pukyong National University, Busan, Korea in 2018. He joined the Faculty of Electronics and Telecommunication, Sai Gon University in 2011 as a lecturer. He has been teaching several undergraduate and graduate courses such as electronic circuits, Automation control theory and Advanced Mathematical Engineering. His current research interests include Control Theory, Power Electronics, and industrial equipment (E-mail: nghhung@sgu.edu.vn).

Van Tu Duong received his B.S. degree from Mechanical Engineering, University of Technical Education Ho Chi Minh City, Vietnam in 2009, his M.S. degree from Mechanical Engineering, Ho Chi Minh City University of Technology, Vietnam in 2012 and his Ph.D. degree in Mechanical Design Engineering, Pukyong National University, Busan, Korea in 2016. His interest includes adaptive Control, manufacturing design, and application control (E-mail: dvtu@hcmut.edu.vn).

Tan Tien Nguyen received his B.S. degree in from Mechanical Engineering, Ho Chi Minh City University of Technology, Vietnam in 1990, his M.S. degree, and his Ph.D. degree in Mechatronics Engineering, Pukyong National University, Busan, Korea in 1998 and 2001, respectively. Since 1990, he has been a lecturer in the Department of Mechanical Design at HCMUT, and since 2005, he has been a lecturer in the Department of Electromechanical Engineering. Since 12.2018, he has held the position of Director of the National Key Laboratory of Digital Control and System Engineering (DCSELab). His current research areas include control theory, robotics and automation, electromechanical systems and their applications in industrial automation (E-mail: nttien@hcmut.edu.vn).